ITF-2003-28
UG-FT-155/03
CAFPE-25/03
hep-ph/0310029
LC-TH-2003-090

CJK- Improved LO Parton Distributions in the Real Photon and Their Experimental Uncertainties

F. Cornet

Departamento de Física Teórica y del Cosmos, Universidad de Granada, Campus de Fuente Nueva, E-18071, Granada, Spain

P. Jankowski and M. Krawczyk

Institute of Theoretical Physics, Warsaw University, ul. Hoża 69, 00-681 Warsaw, Poland

A new analysis of the radiatively generated, LO quark (u, d, s, c, b) and gluon densities in the real, unpolarized photon, improved in respect to our paper [1], is presented. We perform four new global fits to the experimental data for F_2^γ, two using a standard FFNS approach and two based on ACOT_χ scheme [2], leading to the FFNS_{CJK} and CJK models. We also present the analysis of the uncertainties of the new CJK 2 parton distributions due to the experimental errors, the very first such analysis performed for the photon. This analysis is based on the Hessian method, for a comparison for chosen cross-sections we use also the Lagrange method.

CJK- Improved LO Parton Distributions in the Real Photon and Their Experimental Uncertainties

F. Cornet [a], P. Jankowski[b] and M. Krawczyk[b]

[a]Departamento de Física Teórica y del Cosmos, Universidad de Granada,
Campus de Fuente Nueva, E-18071, Granada, Spain

[b]Institute of Theoretical Physics, Warsaw University,
ul. Hoża 69, 00-681 Warsaw, Poland

A new analysis of the radiatively generated, LO quark (u, d, s, c, b) and gluon densities in the real, unpolarized photon, improved in respect to our paper [1], is presented. We perform four new global fits to the experimental data for F_2^γ, two using a standard FFNS approach and two based on ACOT$_\chi$ scheme [2], leading to the FFNS$_{CJK}$ and CJK models. We also present the analysis of the uncertainties of the new CJK 2 parton distributions due to the experimental errors, the very first such analysis performed for the photon. This analysis is based on the Hessian method, for a comparison for chosen cross-sections we use also the Lagrange method.

1. Introduction

We continue our LO analysis [1] of the parton distributions in the unpolarized real photon, which led us to a construction of the CJKL parton parametrization, improving and broadening our investigation. Like previously our aim is to develop a proper description of the heavy charm- and bottom-quark contributions to the photon structure function, $F_2^\gamma(x, Q^2)$. The new models FFNS$_{CJK}$ 1 and CJK 1 are slightly modified versions of our previous FFNS$_{CJKL}$ and CJKL models, respectively. In addition we analyse the FFNS$_{CJK}$ 2 model, which includes the so-called “resolved-photon” contribution of heavy quarks to $F_2^\gamma(x, Q^2)$, given by the $\gamma^* G \to h\bar{h}$ process, and CJK 2 model, with an improved positivity constraint. All models are based on the idea of radiatively generated parton distributions introduced by the GRV group (see e.g. [3]).

In this analysis we neglect TPC2γ data, as in other recent analyses, and slightly modify, with respect to previous analysis, both types of models. Moreover, for the very first time for the photon, we estimate uncertainties of the parton distributions due to the experimental errors of data. Following the analyses of this type performed for proton structure by the CTEQ Collaboration, [4]–[6] and the MRST group, [7] we use the Hessian method to obtain sets of parton parametrizations allowing, along with the parton parametrization of the best fit, to calculate the best estimate and uncertainty of any observable depending on the parton densities in real photon. We compare our results for $F_{2,c}^\gamma$ and prompt photon production in $\gamma\gamma$ obtained with the Hessian and Lagrange ([4],[7], [8]) methods.

2. FFNS$_{CJK}$ and CJK models

The difference between the FFNS$_{CJK}$ and CJK models lays in the approach to the calculation of the heavy quark h (c and b) contributions to the photon structure function $F_2^\gamma(x, Q^2)$. The FFNS$_{CJK}$ models base on a widely adopted Fixed Flavour Number Scheme in which there are no heavy quarks among partons. They contribute to $F_2^\gamma(x, Q^2)$ by a 'direct' (Bethe-Heitler) $\gamma^*\gamma \to h\bar{h}$ process $(F_{2,h}^\gamma(x, Q^2)|_{dir})$, in addition one can also include the so-called 'resolved'-photon contribution from $\gamma^* G \to h\bar{h}$ $(F_{2,h}^\gamma(x, Q^2)|_{res})$ [9]:

$$F_2^\gamma(x, Q^2)|_{FFNS} = x \sum_{i=1}^{3} e_i^2 (q_i^\gamma + \bar{q}_i^\gamma)(x, Q^2) \quad (1)$$

$$+ \sum_{h(=c,b)}^{2} \left[F^{\gamma}_{2,h}(x,Q^2)|_{dir} + F^{\gamma}_{2,h}(x,Q^2)|_{res} \right],$$

with q_i^{γ} ($\bar{q}_i^{\gamma}$) being the light u, d, s quark (anti-quark) densities governed by the DGLAP evolution equations.

The CJK models adopt the ACOT$_{\chi}$ scheme [2] which is a recent realization of the Variable Flavour Number Scheme. In this approach heavy quarks are, similarly to the light quarks, constituents of the photon. Therefore, apart from the direct and resolved-photon contributions also q_h contribute to $F_2^{\gamma}(x,Q^2)$. It leads to a double counting of the heavy quark contributions to $F_2^{\gamma}(x,Q^2)$, therefore inclusion of the corresponding subtraction terms, $F^{\gamma}_{2,h}|_{\rm dir,sub}$ and $F^{\gamma}_{2,h}|_{\rm res,sub}$, is necessary.

Next, following the ACOT$_{\chi}$ approach, we use the χ_h parameters to obtain the proper vanishing of the heavy-quark densities below the kinematic thresholds, for DIS given by the $W^2 = Q^2(1-x)/x = 4m_h^2$. Substitution of x with $\chi_h = x(1 + 4m_h^2/Q^2)$ in q_h and in subtraction terms should lead to the correct threshold behaviour as $\chi_h \to 1$ for $W \to 2m_h$. In the CJK models

$$\begin{aligned} F_2^{\gamma}(x,Q^2)|_{CJK} &= \sum_{i=1}^{3} x e_i^2 (q_i^{\gamma} + \bar{q}_i^{\gamma})(x,Q^2) \qquad (2) \\ &+ \sum_{h(=c,b)}^{2} x e_h^2 (q_h^{\gamma} + \bar{q}_h^{\gamma})(\chi_h,Q^2) \\ + \sum_{h(=c,b)}^{2} &\left[F^{\gamma}_{2,h}(x,Q^2)|_{dir} + F^{\gamma}_{2,h}(x,Q^2)|_{res} \right] \\ &- \sum_{h(=c,b)}^{2} \left[F^{\gamma}_{2,h}|_{\rm dir,sub} + F^{\gamma}_{2,h}|_{\rm res,sub} \right]. \end{aligned}$$

The QCD evolution (DGLAP) starts from a scale chosen to be small, $Q_0^2 = 0.25$ GeV^2, for both types of models, hence our parton densities are radiatively generated. As it is well known the point-like solutions of the evolution equations are calculable without further assumptions, while the hadronic parts need the input distributions. For this purpose we utilize the Vector Meson Dominance (VMD) model, assuming

$$f^{\gamma}_{had}(x,Q_0^2) = \sum_V \frac{4\pi\alpha}{\hat{f}_V^2} f^V(x,Q_0^2) = \kappa \frac{4\pi\alpha}{\hat{f}_\rho^2} f^{\rho}(x,Q_0^2), \qquad (3)$$

where the sum over all light vector mesons (V) is proportional to the ρ^0-meson parton density with a parameter κ. We take the input densities of the ρ meson at Q_0^2 in the form of valence-like distributions both for the (light) quarks (v^{ρ}) and gluons (G^{ρ}):

$$\begin{aligned} xv^{\rho}(x,Q_0^2) &= N_v x^{\alpha}(1-x)^{\beta}, \qquad (4) \\ xG^{\rho}(x,Q_0^2) &= \tilde{N}_g xv^{\rho}(x,Q_0^2) = N_g x^{\alpha}(1-x)^{\beta}, \\ x\zeta^{\rho}(x,Q_0^2) &= 0, \end{aligned}$$

where $N_g = \tilde{N}_g N_v$. All sea-quark distributions (denoted as ζ^{ρ}), including s-quarks, are neglected at the input scale. The valence-quark and gluon densities satisfy the constraint representing the energy-momentum sum rule for ρ:

$$\int_0^1 x(2v^{\rho}(x,Q_0^2) + G^{\rho}(x,Q_0^2))dx = 1. \qquad (5)$$

One can impose an extra constraint related to the number of valence quarks:

$$n_v = \int_0^1 2v^{\rho}(x,Q_0^2) = 2. \qquad (6)$$

Use of both constraints allows to express N_v and N_g in terms of α, β and κ, reducing the number of free parameters to three.

3. New analysis

In our new analysis we improve treatment of the running of α_s by differentiating the number of active quarks in the running of α_s and in the evolution equations, and by using lower values of Λ_{QCD}. We first describe new aspects of our analysis which are common to all considered models.

3.1. Data

New fits were performed using all, $F_2^{\gamma}(x,Q^2)$ data, except the old TPCγ. In our former global analysis [1] we used 208 $F_2^{\gamma}(x,Q^2)$ experimental points. Now we decided to exclude the TPC2γ data (as for instance in [10]) since these data are considered to be not in agreement with other measurements. After the exclusion we have 182 data points.

3.2. α_s running and values of $\Lambda^{(N_q)}$

The running of the strong coupling constant at lowest order is given by the well-known formula:

$$\alpha_s^{(N_q)}(Q^2) = \frac{4\pi}{\beta_0 \ln(Q^2/\Lambda^{(N_q)^2})}, \ \beta_0 = 11 - \frac{2}{3}N_q, \quad (7)$$

where $\Lambda^{(N_q)}$ is the Λ_{QCD} value for N_q quarks. N_q increases by one whenever Q^2 reaches a heavy quark threshold, i.e. when $Q^2 = m_h^2$. The condition $\alpha_s^{(N_q)}(m_h^2) = \alpha_s^{(N_q+1)}(m_h^2)$ is imposed in order to ensure the continuity of the strong coupling constant. In the new analyses we introduce the number of active quarks in the photon, denoted by N_f, which differs from the number of quarks contributing to the running of α_s.

The distinction between both numbers of quarks forces to use slightly more complicated formulae for the evolution of the parton densities than in our previous analysis. More precisely, we must proceed in three steps to perform the DGLAP evolution. In the first step, describing the evolution from the input scale Q_0 to the charm-quark mass m_c, the hadronic input $q^\gamma_{\rm had}(x, Q_0^2)$ is taken from the VMD model. In the second step we evolve the parton distributions from m_c to the beauty-quark mass, m_b, a new hadronic input is given by the sum of already evolved hadronic and point-like contributions to the parton density. The point-like distribution at $Q^2 = m_c^2$ becomes zero again. The same is repeated for $Q^2 > m_b^2$. That way we can solve the equations for three ranges of Q^2, in which $N_f = 3, 4$ and 5, separately. In each range values of b_0 and Λ depend on N_q.

In the previous work we assumed (following the GRV group approach [3]) that the LO and NLO Λ values for four active flavors are equal, and used $\Lambda^{(4)} = 280$ MeV from the Particle Data Group (PDG) report [11]. We now abandon this assumption and take for $\Lambda^{(4)} = 115$ MeV, which is obtained in LO from the world average value $\alpha_s(M_Z) = 0.117$, with $M_Z = 91.188$ GeV, using Eq. 7. Imposing the continuity condition for the strong coupling constant and $m_c = 1.3$ GeV and $m_b = 4.3$ GeV, we obtain $\Lambda^{(3)} = 138$ MeV and $\Lambda^{(5)} = 84$ MeV.

3.3. VDM

In our new analysis we try to relax the constraint on n_v (6). This leads to 4-parameter fit.

3.4. FFNS

In the FFNS$_{CJK}$ 2 model we include the so-called "resolved-photon" contribution of heavy quarks to $F_2^\gamma(x, Q^2)$, given by the $\gamma^* G \to h\bar{h}$ process.

3.5. Subtraction terms in CJK models

In [1] we derived the subtraction term for a direct contribution, $F^\gamma_{2,h}|_{dir,subtr}$, from the integration up to Q^2 of a part of the DGLAP evolution equations, namely:

$$\frac{dq_h^\gamma(x, Q^2)}{d\ln Q^2} = \frac{\alpha}{2\pi} e_h^2 k(x), \quad (8)$$

where $k(x)$ is the lowest order photon-quark splitting function (see Eq. (7) in Ref. [1]). For the lower limit we took in Ref. [1] the natural for a Bethe-Heitler process limit $Q^2_{low} = m_h^2$. However, since the threshold condition is $W^2 \geq 4m_h^2$, even for $Q^2 < m_h^2$ the heavy-quark contributions do not vanish as long as the condition $x < Q^2/(Q^2 + 4m_h^2)$ is fulfilled. In this paper we take $Q^2_{low} = Q_0^2$, which improves quality of the fits. The direct subtraction term has now the form:

$$F^\gamma_{2,h}|_{dir,subtr}(x, Q^2) = x \ln\frac{Q^2}{Q_0^2} 3e_h^4 \frac{\alpha}{\pi}(x^2 + (1-x)^2). \quad (9)$$

We apply the same change to the subtraction term for the resolved-photon contribution:

$$F^\gamma_{2,h}|_{res,subtr} = x \ln\frac{Q^2}{Q_0^2} e_h^2 \frac{\alpha_s(Q^2)}{\pi} \int_x^1 \frac{dy}{y} P_{qG}\left(\frac{x}{y}\right) G^\gamma(y, Q^2). \quad (10)$$

As we noticed in Section 2 the $x \to \chi_h$ substitution leads to the proper threshold behavior of all the heavy-quark contributions to the $F_2^\gamma(x, Q^2)$, except for both subtraction terms. This is already seen in Eq. (9) that this term does not vanish for $\chi_h \to 1$ and therefore by subtracting it the resulting heavy-quark contribution to F_2^γ may become negative for large x. An extra constraint to avoid this unphysical situation is, thus, needed. In Ref. [1] we imposed the simple condition (positivity constraint) that the heavy quark contribution to $F_2^\gamma(x,Q^2)$ has to be positive. Unfortunately, this constraint was not strong enough and for some small windows at small and large x the still unphysical situation $F_{2,h}^\gamma(x,Q^2) < F_{2,h}^\gamma(x,Q^2)|_{direct} + F_{2,h}^\gamma(x,Q^2)|_{resolved}$ was found [12]. In this paper we apply new condition:

$$F_{2,h}^\gamma(x,Q^2) \geq F_{2,h}^\gamma(x,Q^2)|_{dir} + F_{2,h}^\gamma(x,Q^2)|_{res}. \quad (11)$$

4. Results of the new F_2^γ global fits

In the fits we use 182 $F_2^\gamma(x,Q^2)$ experimental points with equal weights. Fits based on the least-squares principle (minimum of χ^2) were done using MINUIT [13]. Systematic and statistical errors on data points were added in quadrature.

The CJK 1 and 2 models differ in the form of the positivity constraint. In the CJK 1 model we keep the old condition $F_{2,h}^\gamma(x,Q^2) > 0$ while the CJK 2 model imposes the condition (11). In these models we do not apply the sum rule (6) and have four free parameters: $\alpha, \beta, N_v, \kappa$ related to the initial quark and gluon densities at the scale $Q_0^2 = 0.25$ GeV^2 (5).

The two FFNS models differ by the resolved-photon contribution of heavy quarks to $F_2^\gamma(x,Q^2)$. It appears only in the FFNS$_{CJK}$ 2 model. In both FFNS models we impose constraints (5) and (6). That allows to write N_v in terms of α, β and κ reducing the number of free parameters to three [1].

The results for the total χ^2 for 182 points and the χ^2 per degree of freedom for our new fits are presented in table 1. The fitted values for parameters α, β, κ and N_v are also presented together with the errors obtained from MINOS program with the standard requirement of $\Delta\chi^2 = 1$. In the case of the FFNS$_{CJK}$ models the N_v parameter is calculated from the constraint (5) and therefore we do not state its error. Note, that the valence number integral n_v (6) gives in CJK models 1.94 and 2.00, for CJK 1 and CJK 2, respectively.

The χ^2 per degree of freedom obtained in our new fits, between 1.5 and 1.7, is better than the old results, mostly due to much lower $\Lambda^{(N_q)}$ as well as due to modification of the subtraction contributions in the CJK models. The old $\chi^2/_{\rm DOF}$ for the same set of 182 data points read 1.99 in the $FFNS_{CJKL}$ and 1.80 in the CJKL model [2].

We observe that the only real difference in $\chi^2/_{\rm DOF}$ is between the first and other three fits and is a result of inclusion or not of the $\gamma^* G \to h\bar{h}$ contribution to $F_2^\gamma(x,Q^2)$. It is obvious that taking this process into account improves the agreement between model and data.

In light of these results one can conclude that in both, so different treatment of heavy-quark contributions to the photon structure function, all fitted parameters are similar. This is related to the fact, that we use in global fits only data for F_2^γ, quantity dominated by the light-quark contributions.

4.1. Comparison with the F_2^γ data

The FFNS$_{CJK}$ 2 and both CJK models predict a much steeper behaviour of the $F_2^\gamma(x,Q^2)$ at small x with respect to FFNS$_{CJK}$ 1 fit and GRS LO [14] and SaS1D [15] parametrizations. On the other hand these curves are less steep than the FFNS$_{CJKL}$ and CJKL results from [1]. In the region of $x \gtrsim 0.1$, the behaviour of the $F_2^\gamma(x,Q^2)$ obtained from all fits and parametrizations apart from the CJK 1 model is similar. The shape of the CJK 1 fit at high x is a result of the $F_{2,h}^\gamma(x,Q^2) > 0$ condition which allows for $F_{2,h}^\gamma(x,Q^2) < F_{2,h}^\gamma(x,Q^2)|_{direct} + F_{2,h}^\gamma(x,Q^2)|_{resolved}$. It effects in the lower position of the characteristic point at which the charm-quark contributions to the $F_2^\gamma(x,Q^2)$ appear as compared to other models predictions. Apart from that the CJK 1 fit gives smaller $F_2^\gamma(x,Q^2)$ values around this charm-quark threshold. Finally at high Q^2 and high x the CJK 1 model produces much lower structure function values than all other fits and parametrizations predict. We found that the FFNS$_{CJK}$ 1 fit gives very similar prediction to the GRS LO parametrization results in the whole range of x.

Figure 1 presents the predictions for $F_2^\gamma(x,Q^2)$,

[1]The test fits without the number of valence quarks constraint gave $n_v \approx 0.5$ and ≈ 1.4 in the FFNS$_{CJK}$ 1 and FFNS$_{CJK}$ 2 models, respectively. Both these values are very far away from the expected value 2.

[2]Note, however that in old analysis global fits were performed for 208 points.

model	χ^2 (182 pts)	χ^2/DOF	κ	α	β	N_v	$\tilde{N}_g$
FFNS$_{CJK}$ 1	314.0	1.754	$2.267^{+0.063}_{-0.072}$	$0.265^{+0.038}_{-0.032}$	$0.792^{+0.189}_{-0.149}$	0.358	5.02
FFNS$_{CJK}$ 2	279.8	1.563	$2.110^{+0.084}_{-0.090}$	$0.310^{+0.054}_{-0.051}$	$0.823^{+0.265}_{-0.223}$	0.415	4.51
CJK 1	273.9	1.539	$2.146^{+0.154}_{-0.144}$	$0.218^{+0.070}_{-0.063}$	$0.462^{+0.261}_{-0.227}$	$0.269^{+0.076}_{-0.059}$	5.00
CJK 2	273.7	1.537	$1.934^{+0.131}_{-0.124}$	$0.299^{+0.077}_{-0.069}$	$0.898^{+0.316}_{-0.275}$	$0.404^{+0.116}_{-0.088}$	4.93

Table 1
The total χ^2 for 182 data points and per the degree of freedom, and parameters of the best fits for FFNS$_{CJK}$ and CJK models. Errors are obtained from MINOS with $\Delta\chi^2 = 1$.

averaged over medium x regions, compared with the recent OPAL data [16], not used directly in our analysis. Like in our previous analysis we see that all FFNS type predictions (including GRS LO and SaS1D parametrizations) are similar and fairly well describe the experimental data. The CJK models alike the CJKL model gives slightly better agreement with the data.

4.2. Parton densities

The parton densities obtained in the CJK and FFNS$_{CJK}$ models are all very similar. Of course there are no heavy-quark distributions in FFNS models. In case of the CJK models the $c^\gamma(x,Q^2)$ and $b^\gamma(x,Q^2)$ densities vanish not at $x=1$, as for the GRV LO and SaS1D parametrizations, but at the kinematical threshold, which was our aim. We notice that our new parton densities have all similar shapes but slightly higher values than the corresponding old CJKL distributions. In case of the gluon density we find that all new curves are much steeper than the predictions of the old models and the GRV LO and SaS1D parametrizations, see also below.

4.3. Comparison with $F_{2,c}^\gamma$

In Fig. 2 we present our predictions for the $F_{2,c}^\gamma$, in comparison with OPAL data [17], not used directly in the analysis, and results of the GRS LO and SaS1D parametrizations.

All our models containing the resolved-photon contribution (FFNS$_{CJK}$ 2 and both CJK models) agree better with the low x experimental point than other predictions. The GRS LO and SaS1D parametrizations also include the resolved-photon term but in their case the gluon density increased less steep than our models predict, as was already mentioned. Their $F_{2,c}^\gamma$ lines lie below results of our new fits but higher than the FFNS$_{CJK}$ 1 curve which is given solely by the direct Bethe-Heitler contribution.

The CJK models overshoot the experimental point at high x while other predictions agree with it within its uncertainty bounds. Again the $F_{2,c}^\gamma$ from the CJK 1 fit vanishes at lower x than in other models.

5. Uncertainties of the parton distributions

Following the corresponding analyses for the proton we consider the experimental uncertainties of the CJK parton densities. This is first analysis of this type for the photon, details are described in [18].

5.1. The Hessian method

The CTEQ Collaboration [4]-[6], developed and applied an improved method of the treatment of the experimental data errors. Later the same formalism has been applied by the MRST group in [7]. The method bases on the Hessian formalism and as a result one obtains a set of parametrizations allowing for the calculation of an uncertainty of any physical observable depending on the parton densities.

We apply the method as described in Refs. [4] and [5]. For the sake of clearness of our procedures we will partly repeat it here keeping the notation introduced by the CTEQ Collaboration.

Let us consider a global fit to the experimental data based on the least-squares principle performed in a model, being parametrized with a

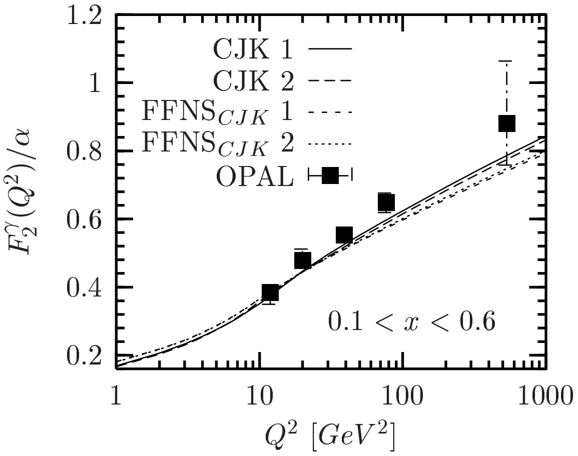

Figure 1. Comparison of the recent OPAL data [16] for the Q^2-dependence of the averaged over $0.1 < x < 0.6$ F_2^γ/α with the predictions of the CJK and FFNS$_{CJK}$ models.

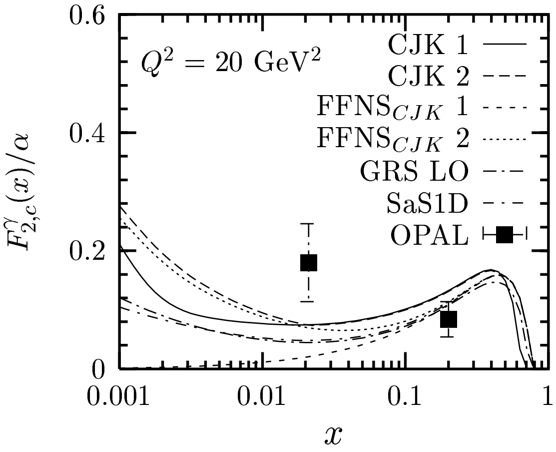

Figure 2. Comparison of the structure function $F_{2,c}^\gamma(x,Q^2)/\alpha$ calculated in the CJK and FFNS$_{CJK}$ models and in GRS LO [14] and SaS1D [15] parametrizations with the OPAL data [17].

set of $\{a_i, i = 1, 2, \cdots d\}$ parameters. Each set of values of these parameters constitutes a test parametrization S. The set of the best values of parameters $\{a_i^0\}$, corresponding to the minimal χ^2, χ_0^2, is denoted as S^0 parametrization. In the Hessian method one makes a basic assumption that the deviation of the global fit from χ_0^2 can be approximated in its proximity by a quadratic expansion in the basis of parameters $\{a_i\}$

$$\Delta\chi^2 = \chi^2 - \chi_0^2 = \sum_{i=1}^{d}\sum_{j=1}^{d} H_{ij}(a_i - a_i^0)(a_j - a_j^0), \quad (12)$$

where H_{ij} is an element of the Hessian matrix, calculated as

$$H_{ij} = \frac{1}{2}\left(\frac{\partial^2\chi^2}{\partial a_i \partial a_j}\right)_{a_0}. \quad (13)$$

Since the H_{ij} is a symmetric matrix, it has a complete set of $k = 1, 2...d$ orthonormal eigenvectors $(v_i)_k$ defined by

$$\sum_{j=1}^{d} H_{ij}(v_j)_k = \epsilon_k (v_i)_k, \quad (14)$$

$$\sum_{i=1}^{d} (v_i)_j (v_i)_k = \delta_{jk}, \quad (15)$$

with $\{\epsilon_k\}$ being the corresponding eigenvalues. Variations around the minimum can be expressed in terms of the basis provided by the set of eigenvectors

$$a_i - a_i^0 = \sum_{k=1}^{d} s_k z_k (v_i)_k, \quad (16)$$

where $\{z_k\}$ are new parameters describing the displacement from the best fit. The $\{s_k\}$ are scale factors introduced to normalize $\{z_k\}$ in such a way that

$$\Delta\chi^2 = \chi^2 - \chi_0^2 = \sum_{k=1}^{d} z_k^2. \quad (17)$$

The above equation means that the surfaces of constant χ^2 are spheres in the $\{z_k\}$ space. That way the $\{z_k\}$ coordinates create a very useful, normalized basis. The $(v_i)_k \equiv v_{ik}$ matrix describes the transformation between this new basis $\{z_k\}$ and old $\{a_i\}$ basis. The scaling factors s_k are equal to $\sqrt{1/\epsilon_k}$ in the ideal quadratic approximation (13).

The Hessian matrix can be calculated from its definition in Eq. (13). Such computation meets many practical problems arising from the large range spanned by the eigenvalues $\{\epsilon_k\}$, the numerical noise and non-quadratic contributions to χ^2. The solution (an iteration procedure) has been given by the CTEQ Collaboration [4].

Having calculated the eigenvectors, eigenvalues and scaling factors we can create a basis of the parametrizations of the parton densities, $\{S_k^{\pm}, k = 1, \cdots, d\}$. Each parametrization corresponds to a k-set of a_i parameters defined by displacements from a_i^0 of a magnitude t "up" or "down" along the corresponding eigenvector direction

$$a_i(S_k^{\pm}) = a_i^0 \pm t\,(v_i)_k s_k. \tag{18}$$

For each $S_k^{\pm}$ parametrization $\Delta\chi^2 = t^2$.

The best value of a physical observable X depending on the photon parton distributions is given as $X(S^0)$. The uncertainty of X, for a displacement from the parton densities minimum by $\Delta\chi^2 = T^2$ (T - the tolerance parameter), can be calculated from a very simple expression (a master equation)

$$\Delta X = \frac{T}{2t}\left(\sum_{k=1}^{d}[X(S_k^+) - X(S_k^-)]^2\right)^{\frac{1}{2}}. \tag{19}$$

Note that having calculated ΔX for one value of the tolerance parameter T we can obtain the uncertainty of X for any other T by simple scaling of ΔX. This way sets of $\{S_k^{\pm}\}$ parton densities give us a perfect tool for studying of the uncertainties of other physical quantities. One of such quantities can be the parton densities themselves.

Finally, we can calculate the uncertainties of the a_i parameters of the model. According to Eq. (18) in this case $a_i(S_k^+) - a_i(S_k^-) = 2t(v_i)_k s_k$ and the master equation gives a simple expression

$$\Delta a_i = T\left(\sum_{k=1}^{d} v_{ik} s_k\right)^{\frac{1}{2}}. \tag{20}$$

In practice we observe the considerable deviations from the ideal quadratic approximation of equation (17). To make an improvement we can adjust the scaling factors $\{s_i\}$ either to obtain exactly $\Delta\chi^2 = t^2$ at $z_i = t$ for each of the $S_i^{\pm}$ sets or to get the best average agreement over some z_i range (for instance for $z_i \le t$). Below we apply the second approach.

5.1.1. Estimate of the tolerance parameter T for the photon densities

We consider now the value of the tolerance parameter T for the real-photon parton-densities corresponding to the allowed deviation of the global fit from the minimum, $\Delta\chi^2 = T^2$, as described above. In case of an ideal analysis a standard requirement is $\Delta\chi^2 = 1$. Of course this is not a case for a global fit to the F_2^{γ} data coming from various experiments, and certainly T must be greater than 1. Unfortunately, no strict rules allowing for estimation of the tolerance parameter exist, as discussed in detail in [5] and [8]. We try to estimate the reliable T value in two ways, both applied to the CJK 2 fit only.

First we examine the mutual compatibility of the experiments used in the fit. That gives the allowed $\Delta\chi^2$ greater than 22 and the tolerance parameter $T \sim 5$. As a second test we compare the results of our four fits presented in this paper and find the T values for which parton densities predicted by the FFNS and CJK 1 models lie between the lines of uncertainties of the CJK 2 model. These values are large due to the differences between the gluon densities given by the CJK and FFNS models. The $T \sim 5$ when only the CJK 1 and 2 gluon distributions are compared. For quark distributions $T \le 7$ when we consider all models. Finally we estimate that the tolerance parameter T should lie in the range $5 \sim 10$.

5.1.2. Tests of quadratic approximation

For each CJK model we obtained a set of the $\{(v_i)_k\}$ and $\{s_k\}$ values, with i and $k = 1, \cdots, 4$ (since $d = 4$ in CJK models). We used the iteration procedure from [4]. Further we adjusted the scaling factors $\{s_k\}$ to improve the average quadratic approximation over the $z_k \le 5$ range.

Further we check if the quadratic approximation on which the Hessian method relies is valid in the considered $\Delta\chi^2$ range for the CJK 2 model (for the CJK 1 model results are similar). In the left panel of Fig. 3 we present the comparison of the χ^2 dependence along each of four eigenvector directions (for the eigenvector k $z_i = \delta_{ik}$) with the dependence of the ideal $\Delta\chi^2 = z_i^2$ curve. Only the line corresponding to the eigenvector 4 does not agree with the theoretical prediction. More-

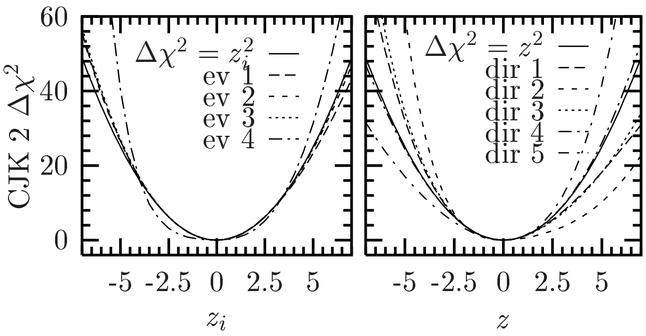

Figure 3. CJK 2 model. The left plot presents a comparison of the χ^2 dependence along each of the four eigenvector directions to the ideal $\Delta\chi^2 = z_i^2$ curve. In right plot analogous comparison for five random directions in $\{z_i\}$ space are shown. The ideal curve corresponds to $\Delta\chi^2 = \sum z_i^2 = z^2$

over it has a different shape than other lines which results from the scaling adjustment procedure. In the right panel of Fig. 3 an analogous comparison for the five randomly chosen directions in the $\{z_i\}$ space is shown. For each of directions $\sum_{k=1}^{d} z_k^2 = z^2$ and the ideal curve corresponds to $\Delta\chi^2 = z^2$. In this case we observe greater deviations from the quadratic approximation.

5.1.3. CJK 1 and CJK 2 parametrizations

The errors calculated within the Hessian quadratic approximation are shown in table 2 for the standard requirement of $\Delta\chi^2 = 1$. They should be compared with the slightly smaller errors calculated by MINUIT and shown in table 1.

All parton distributions are further parametrized on a grid. The resulting programs can be found on the web-page [19].

5.1.4. Uncertainties of the CJK 2 parton densities

In this section we discuss the uncertainties of the CJK 2 parton densities, the results obtained with CJK 1 model are very similar.

In Figure 4 the up, strange and charm-quark and gluon densities calculated in FFNS_{CJK} and CJK 1 models are compared with the CJK 2 predictions. We plot the

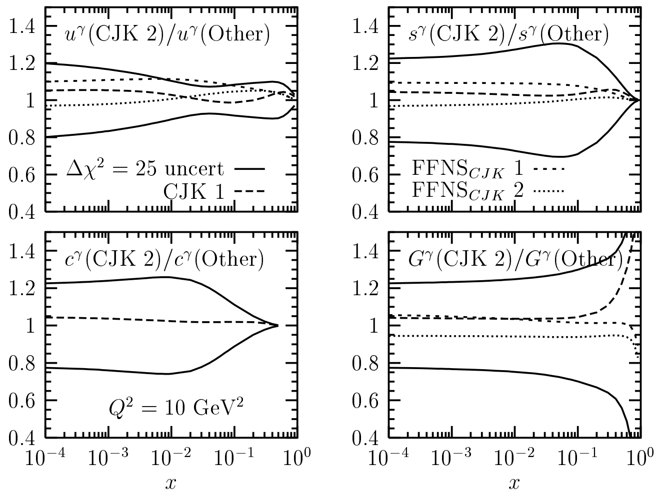

Figure 4. Parton densities calculated in FFNS_{CJK} and CJK 1 models compared with the CJK 2 predictions. We plot for $Q^2 = 10$ the $q^\gamma(\mathrm{CJK2})/q^\gamma(\mathrm{Other})$ ratios of parton densities. Solid lines show the CJK 2 fit uncertainties for $\Delta\chi^2 = 25$.

$q^\gamma(\mathrm{CJK\,2})/q^\gamma(\mathrm{Other\ models})$ ratios of the parton q^γ densities calculated in the CJK 2 model to their values obtained with other models for $Q^2 = 10$. Solid lines show the CJK 2 fit uncertainties for $\Delta\chi^2 = 25$ computed with the $\{S_k^\pm\}$ parametrizations.

First we notice that predictions of all our models for all considered parton distributions lie between the lines of the CJK 2 uncertainties. This indicates that the choice of $\Delta\chi^2 = 25$ agrees with the differences among our four models. We found, that the SaS1D results differ very substantially from the CJK 2 ones (not shown).

As expected the up-quark distribution is the one best constrained by the experimental data while the greatest uncertainties are for the gluon densities. In the case of u^γ the $\Delta\chi^2 = 25$ band widens in the small x region. Alike in the case of s- and c-quark uncertainties it shrinks at high x. On contrary the gluon distributions are least constrained at the region of $x \to 1$. All uncertainties become slightly smaller for higher Q^2.

model	κ	α	β	N_v
CJK 1	$2.146^{+0.120}_{-0.107}$	$0.218^{+0.054}_{-0.047}$	$0.462^{+0.157}_{-0.126}$	$0.269^{+0.041}_{-0.035}$
CJK 2	$1.934^{+0.112}_{-0.103}$	$0.299^{+0.061}_{-0.051}$	$0.898^{+0.204}_{-0.156}$	$0.404^{+0.066}_{-0.054}$

Table 2
The parameters of the fits for CJK models with errors calculated in the Hessian quadratic approximation for the standard requirement of $\Delta\chi^2 = 1$

5.2. Lagrange method for the uncertainties of the parton distributions

The Hessian method allows the computation of the parton density uncertainties in a very simple and effective way. However, the Hessian method relies on the assumption of the quadratic approximation, which as we have shown in the former section, is not perfectly preserved.

There exist another method called the Lagrange multiplier method which allows to find exact uncertainties independently on the quadratic approximation (for the proton structure used in [4],[7] and [8]). In this approach one makes a series of fits on the quantity

$$F(\lambda, \{a_i\}) = \chi^2(\{a_i\}) + \lambda X(\{a_i\}), \qquad (21)$$

each with a different but fixed value of the Lagrange multiplier λ. As a result one obtains a set of points $(\chi^2(\lambda), X(\lambda)$ which characterize the deviation of the physical quantity X from its best value X_0, for a corresponding deviation of the structure function global fit from its minimum $\Delta\chi^2 = \chi^2(\lambda) - \chi_0$. In each of this constrained (by the λ parameter) fits we find the best value of X and the optimal χ^2. For $\lambda = 0$ we return to the basic fit which gives $\{a_i^0\}$ parameters and allows to calculate the best X_0 value. The great advantage of this approach lies in the fact that we do not assume anything about the uncertainties. The large computer time consuming of the process of the whole series of minimalizations is a huge disadvantage of the Lagrange method.

5.3. Examples of cross-section uncertainties in Hessian and Lagrange methods

Finally we made a comparison of the uncertainties obtained for the CJK 2 model in Hessian and Lagrange methods for two physical quantities. For the sake of limitation of the computer time we chose two very simple examples: $F_{2,c}^{\gamma}$ points measured by the OPAL Collaboration [17] and the $\gamma q \to \gamma q$ part of the cross-section for prompt photon production in $\gamma\gamma$. Results for the later case are presented in Fig. 5.

6. Summary

We enlarged and improved our previous analysis [1]. We performed new global fits to the $F_2^{\gamma}(x, Q^2)$ data. Two additional models were analysed. New fits gave χ^2 per degree of freedom, 1.5-1.7, about 0.25 better than the old results. All features of the CJKL model, such as heavy-quark distributions, good description of the LEP data on the Q^2 dependence of the F_2^{γ} and on $F_{2,c}^{\gamma}$ are preserved. We checked that the gluon densities of our models agree with the H1 measurement of the G^{γ} distribution performed at $Q^2 = 74$ GeV^2 [20], Fig. 6. [3]

An analysis of the uncertainties of the CJK parton distributions due to the experimental errors based on the Hessian method was performed for the very first time for the photon. We constructed sets of test parametrizations for both CJK models. They allow to computate uncertainties of any physical quantity depending on the real photon parton densities.

Parametrization programs for all models can be obtained from the web-page [19].

7. Acknowledgment

This work was partly supported by the European Community's Human Potential Programme

[3] Further comparison of our gluon densities to the H1 data cannot be performed in a fully consistent way, since the GRV LO proton and photon parametrization were used in the experiment in order to extract such gluon density.

under contract HPRN-CT-2000-00149 Physics at Collider and HPRN-CT-2002-00311 EURIDICE.

REFERENCES

1. F. Cornet, P. Jankowski, M. Krawczyk and A. Lorca, Phys. Rev. **D68** 014010 (2003)
2. S. Kretzer, C. Schmidt and W. Tung, J. Phys. **G28**, 983 (2002)
3. M. Glück, E. Reya and A. Vogt, Phys. Rev. **D46**, 1973 (1992)
4. J. Pumplin, D.R. Stump and W.K. Tung, Phys. Rev. **D65**, 014011 (2002)
5. J. Pumplin *et al.*, Phys. Rev. **D65**, 014013 (2002)
6. J. Pumplin *et al.*, JHEP 0207, 012 (2002)
7. A.D. Martin, R.G. Roberts, W.J. Stirling and R.S. Thorne, Eur. Phys. J. **C28**, 455 (2003)
8. D. Stump *et al.*, Phys. Rev. **D65**, 014012 (2002)
9. M.Glück, E.Reya and M.Stratmann, Phys. Rev. **D51**, 3220 (1995)
10. S. Albino, M. Klasen and S. Söldner-Rembold, Phys. Rev. Lett. **89**, 122004 (2002).
11. Particle Data Group (D.E. Groom *et al.*), Eur. Phys. J. **C15**, 1 (2000)
12. We thank Mariusz Przybycień for pointing this problem to us.
13. F. James and M. Roos, Comput. Phys. Commun. **10**, 343 (1975)
14. M. Glück, E. Reya and I. Schienbein, Phys. Rev. **D60**, 054019 (1999), Erratum-ibid. **D62**, 019902 (2000)
15. G.A. Schuler and T. Sjöstrand, Z. Phys. **C68**, 607 (1995); Phys. Lett. **B376**, 193 (1996)
16. OPAL Collaboration, G. Abbiendi *et al.*, Phys. Lett. **B533**, 207 (2002).
17. OPAL Collaboration, G. Abbiendi *et al.*, Phys. Lett. **B539**, 13 (2002)
18. P. Jankowski PhD thesis, and F. Cornet, P. Jankowski, M. Krawczyk, in preparation
19. http://www.fuw.edu.pl/~pjank/param.html
20. H1 Collaboration, C. Adloff *et al.*, Phys. Lett. **B483**, 36 (2000)

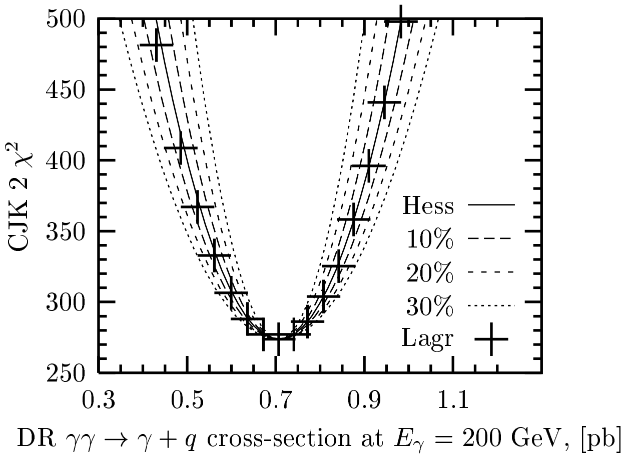

Figure 5. CJK 2 model. Lagrange and Hessian method results for the direct resolved (DR) part of the $\gamma\gamma \to \gamma q$ cross-section. The dashed lines represent the 10 to 30% deviation from the Hessian result.

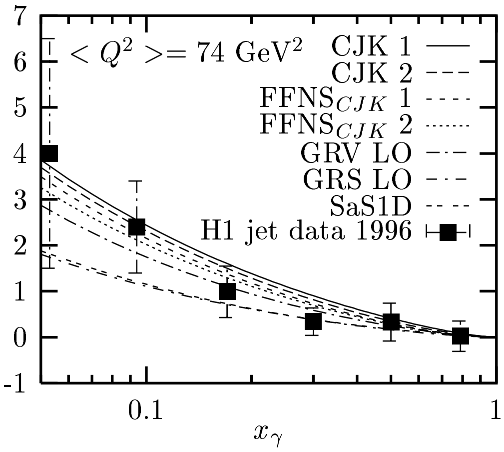

Figure 6. Comparison of the gluon distribution obtained in the H1 measurement performed at $Q^2 = 74$ GeV^2 [20] with the predictions of the CJK, FFNS$_{CJK}$ models and GRV LO [3], GRS LO [14] and SaS1D [15] parametrizations with the OPAL measurement [17].